Title

Accumulation, internalization and therapeutic efficacy of neuropilin-1-targeted liposomes

Journal

Journal of Controlled Release, 178(1)

ISSN

0168-3659

Authors

Paoli, Eric E
Ingham, Elizabeth S
Zhang, Hua
et al.

Publication Date

2014-03-01

DOI

10.1016/j.jconrel.2014.01.005

Peer reviewed

Published in final edited form as:
J Control Release. 2014 March 28; 178: 108–117. doi:10.1016/j.jconrel.2014.01.005.

Accumulation, internalization and therapeutic efficacy of neuropilin-1-targeted liposomes

Eric E. Paoli, **Elizabeth S. Ingham**, **Hua Zhang**, **Lisa M. Mahakian**, **Brett Z. Fite**, **M. Karen Gagnon**, **Sarah Tam**, **Azadeh Kheirolomoom**, **Robert D. Cardiff**, and **Katherine W. Ferrara***
University of California, Davis, Department of Biomedical Engineering, 451 Health Sciences Drive, Davis, CA 95616

Eric E. Paoli: eepaoli@ucdavis.edu; Elizabeth S. Ingham: esingham@ucdavis.edu; Hua Zhang: hchzhang@ucdavis.edu; Lisa M. Mahakian: lmmahakian@ucdavis.edu; Brett Z. Fite: bzfite@ucdavis.edu; M. Karen Gagnon: mkgagnon@ucdavis.edu; Sarah Tam: smjohns@ucdavis.edu; Azadeh Kheirolomoom: akheirolomoom@ucdavis.edu; Robert D. Cardiff: rdcardiff@ucdavis.edu

Abstract

Advancements in liposomal drug delivery have produced long circulating and very stable drug formulations. These formulations minimize systemic exposure; however, unfortunately, therapeutic efficacy has remained limited due to the slow diffusion of liposomal particles within the tumor and limited release or uptake of the encapsulated drug. Here, the carboxyl-terminated CRPPR peptide, with affinity for the receptor neuropilin-1 (NRP), which is expressed on both endothelial and cancer cells, was conjugated to liposomes to enhance the tumor accumulation. Using a pH sensitive probe, liposomes were optimized for specific NRP binding and subsequent cellular internalization using *in vitro* cellular assays. Liposomes conjugated with the carboxyl-terminated CRPPR peptide (termed C-LPP liposomes) bound to the NRP-positive primary prostatic carcinoma cell line (PPC-1) but did not bind to the NRP-negative PC-3 cell line, and binding was observed with liposomal peptide concentrations as low as 0.16 mol%. Binding of the C-LPP liposomes was receptor-limited, with saturation observed at high liposome concentrations. The identical peptide sequence bearing an amide terminus did not bind specifically, accumulating only with a high (2.5 mol%) peptide concentration and adhering equally to NRP positive and negative cell lines. The binding of C-LPP liposomes conjugated with 0.63 mol% of the peptide was 83-fold greater than liposomes conjugated with the amide version of the peptide. Cellular internalization was also enhanced with C-LPP liposomes, with 80% internalized following 3hr incubation. Additionally, fluorescence in the blood pool (~40% of the injected dose) was similar for liposomes conjugated with 0.63 mol% of carboxyl-terminated peptide and non-targeted liposomes at 24 hr after injection, indicating stable circulation. Prior to doxorubicin treatment, *in vivo* tumor accumulation and vascular targeting were increased for peptide-conjugated liposomes compared to non-targeted liposomes based on confocal imaging of a fluorescent cargo, and the

Corresponding author: Katherine W. Ferrara, One Shields Avenue, Department of Biomedical Engineering, UC Davis, Davis CA 95616, USA, (530)754-9436, FAX (530)754-5739, kwferrar@ucdavis.edu.

availability of the vascular receptor was confirmed with ultrasound molecular imaging. Finally, over a 4-week course of therapy, tumor knockdown resulting from doxorubicin-loaded, C-LPP liposomes was similar to non-targeted liposomes in syngeneic tumor-bearing FVB mice and C-LPP liposomes reduced doxorubicin accumulation in the skin and heart and eliminated skin toxicity. Taken together, our results demonstrate that a carboxyl-terminated RXXR peptide sequence, conjugated to liposomes at a concentration of 0.63 mol%, retains long circulation but enhances binding and internalization, and reduces toxicity.

Keywords

Doxorubicin; Toxicity; CendR; Neuropilin-1; Liposome; Optical Imaging

1. Introduction

There are four requirements that are essential for effective liposomal drug delivery: stable circulation, immune evasion, target retention and release or internalization of the drug payload [1]. Prior to the use of lipid-tethered polyethylene glycol (PEG), conventional liposomes were rapidly cleared from the blood of rats [2]. While PEG incorporation has increased plasma circulation times, therapeutic efficacy has not increased in proportion to the enhanced circulation [3]. The limited efficacy results in part from the slow diffusion of liposomal particles within the tumor and limited release or uptake of the encapsulated drug [4, 5].

Ligands have been incorporated onto the surface of liposomes in an effort to target cellular receptors and specifically deliver the liposomal cargo to vascular and tumor cell surface receptors [6]. While many targeted liposomes show great promise *in vitro*, most *in vivo* studies report minimal improvements in efficacy [7]. In part, targeted drug delivery remains challenging due to the increased immunogenicity of targeted drug carriers bearing surface ligands [8]. Recently, synthetic peptides have been incorporated as liposomal targeting moieties due to their decreased immunogenicity. Multivalent presentation of a peptide on a nanoparticle provides high avidity for the target. Additionally, peptide synthesis is relatively simple and phage libraries can be applied to identify sequences that accumulate in specific tissues.

Teesalu et al. have recently applied phage screening to identify the peptide sequence RXXR containing a C-terminal arginine with a free carboxyl group as a ligand for neuropilin-1 (NRP) [9]. NRP expression is up-regulated in multiple tumor types as well as on tumor vasculature [10–13]. Further, ligands containing the peptide sequence R/K-XX-R/K that terminate with a C-terminal carboxyl group, have been shown to enhance cellular penetration and have been designated as following the C-end Rule (CendR). The RXXK/R sequence is also embedded within the iRGD peptide, where the cyclic peptide is thought to be cleaved within the tumor to produce a CendR peptide [14]. In this study, we evaluate the circulation and efficacy of liposomes conjugated with the linear peptide CRPPR. CRPPR, containing a C-terminal amide, has previously been reported by our group and others to specifically target the heart endothelium [15–17]. Here, we compare the affinity of

liposomes conjugated with CRPPR which contains a C-terminal carboxyl group with that of liposomes conjugated with CRPPR containing a C-terminal amide in the targeting of NRP-positive and NRP-negative cell lines and a mouse tumor with angiogenic vasculature.

Cellular uptake of liposomes is generally believed to be mediated by adsorption of liposomes onto the cell surface, followed by endocytosis through a coated pit-mediated pathway [18]. Recent findings with CendR suggest involvement of a distinct pathway thought to involve pinocytosis and hypothesized to be exocytic [9, 14]. Here, we utilize a pH-dependent fluorophore (HPTS) encapsulated in liposomes that emits maximally at 510 nm after excitation at 450 nm in neutral media or 403 nm in acidic media to monitor the intracellular fate of liposomes [19].

In addition, *in vivo* small animal optical imaging techniques allow for sensitive detection of liposomal stability and accumulation of a model drug over 24 hr. Ultrasound molecular imaging facilitates estimation of vascular receptor density [20]. Encapsulating a quenched near-infrared fluorophore within a liposome and measuring the resulting superficial fluorescence in specified regions of interest (ROIs) facilitates immediate visualization of cargo leakage through fluorophore dequenching [21]. The chemotherapeutic drug doxorubicin (Dox) can also be actively loaded into liposomes and internalization and accumulation can also be validated using small animal optical imaging. Dox is a frequently used chemotherapeutic where cardiomyopathy has been demonstrated when free Dox doses exceed 550 mg/m^2 [22]. Encapsulation of Dox is desirable to reduce toxicity and enhance efficacy, yet few studies have evaluated the use of targeted therapies over a multi-week course of treatment. In this study, we apply animal imaging techniques to evaluate the accumulation and vascular targeting *in vitro* and *in vivo* in a mouse model of cancer. Our overall goal is to design an optimized targeted delivery system for Dox using a CendR peptide at a low concentration to enhance accumulation and internalization.

2. Materials and Methods

2.1. Liposome preparation and Dox loading

All chemicals were purchased from Sigma Chemical Co. (St. Louis, MO) unless otherwise specified. The following five aqueous solutions were used to re-suspend the dried lipid films: 1) 10 mM 8-hydroxy-1,3,6 pyrene trisulfonate (HPTS) in 5 mM tris(hydroxymethyl)aminomethane (TRIS) buffered saline; 2) 25 mM bis-1,1’-(4-sulfobutyl)-indotricarbocyanine-5,5’-dicarboxylic acid (SIDA, synthesized as in [23]) in Dulbecco's phosphate-buffered saline (DPBS, Invitrogen, Carlsbad, CA); 3) gadolinium complex of 10-(2-hydroxy-propyl)-1,4,7,10- tetraazacyclododecane-1,4,7-triacetic acid in 10 mM TRIS and 477 μM calteridol calcium (Prohance, Bracco Diagnostics Inc., Princeton, NJ), diluted with equal volume of ddH_2O; 4) 250 mM ammonium sulfate (552 mOsm); and 5) 2mM Alexa 555 in DPBS. For active Dox loading, 10% sucrose in 20 mM 4-(2-hydroxyethyl)-1-piperazineethanesulfonic acid (HEPES) (SH buffer) was prepared, and a Dox stock solution (10 mg/ml in ddH_2O) was used. All of the solutions, except ammonium sulfate and Dox solutions, were adjusted with NaOH or HCl to reach pH 7.5 and 295 mOsm.

1,2-distearoyl-sn-glycero-3-phosphoethanolamine-N-[methoxy(polyethyleneglycol)-2000] (DSPE-PEG2k), L-α-phosphatidylcholine (hydrogenated-SoyPC, HSPC), cholesterol (Chol), and a mini-extruder were purchased from Avanti Polar Lipids (Alabaster, AL) and all of the lipids were stored at −20°C in chloroform. Two lipo-PEG-peptides (LPP), synthesized as in [15] to give the dimerized CRPPR-LPP, were prepared; however, one was prepared such that it contained a C-terminal amide (A-LPP), while the other contained a C-terminal carboxylic acid (C-LPP).

HPTS-, SIDA-, Prohance- and ammonium sulfate-containing liposomes were prepared by lipid film hydration, freeze/thaw and extrusion as previously described [21, 24] with some modifications. Briefly, lipids dissolved in chloroform were mixed at the desired molar ratios, dried into a thin film under a gentle stream of nitrogen and subsequently lyophilized overnight. The dried lipid film was rehydrated in the desired solution and warmed at 55°C for 1 hr with gentle vortexing every 10 min. The resultant multilamellar lipid vesicles were subsequently frozen in liquid nitrogen and thawed in a 65°C water bath (freeze/thaw) 5 times with intense vortexing between freeze/thaws. The solution was then extruded 41 times through a 100 nm polycarbonate filter at 65°C, and the liposomes were purified with a gel filtration column (Sephadex G-75, GE Healthcare, NJ) equilibrated with DPBS or SH buffer (only for Dox loading). Alexa 555-loaded liposomes were made similarly except that freeze/thaw cycles were not required.

Dox active loading was performed as previously reported [25] with slight modifications. Briefly, ammonium sulfate-containing liposomes at a concentration of 10 mg/ml in SH buffer were heated to 60°C and the Dox solution was added at a drug to lipid weight ratio of 0.2:1 and incubated for 1hr. The un-encapsulated Dox was then separated from the liposome vesicles by a second round of gel filtration using a Sephadex G-75 column equilibrated with PBS buffer.

Liposome size was verified using a Nicomp 380 submicron particle analyzer (Santa Barbara, CA). The mean liposomal diameters observed for non-targeted (NT) and targeted liposomes were 97.4±8.8 nm and 124.5±32.4 nm, respectively. The phospholipid concentration was tested with the Phospholipid C Kit from Wako Chemical USA, Inc. (Richmond, VA). Fluorometric analysis validated both dye encapsulation and Dox loading efficiencies. For each liposomal formulation, the aqueous cargo concentrations were matched. Liposomes were prepared on a weekly basis and stored at 4°C.

2.2. Cell experiments

Two prostate cancer cell lines, primary prostate carcinoma-1 (PPC-1, positive for NRP expression) and PC-3 (negative for NRP expression), were used in this study. The PPC-1 cell line was a generous gift from Dr. Arthur Brothman (University of Utah, School of Medicine), and PC-3 cells were obtained from ATCC (Manassa, VA). NRP expression was verified with the NRP antibody (Supplementary Information). The cells were grown to 70–75% confluency in 75 cm^2 flasks in DMEM high glucose media (for PPC-1, from Invitrogen, Carlsbad, CA) or phenol red-free DMEM (for PC-3, from Sigma Aldrich, St. Louis, MO) supplemented with 1% penstrep and 10% FBS in an incubator maintained with 5% CO_2 at 37°C. Then, the cells were detached using TrypLE Express (Invitrogen,

Carlsbad, CA), centrifuged at 100 × g 5 min, the supernatant was removed and the cells were resuspended in media and transferred to 35-mm culture dishes or 96-well culture plates 48 hr prior to experiments.

2.2.1. Binding and internalization of liposomes studied by loading a pH sensitive fluorophore—Liposome binding and internalization were studied by encapsulating a hydrophilic fluorescent molecule, HPTS, where the fluorescence measured at 510 nm is pH insensitive when excited at 413 nm, or pH sensitive when excited at 450 nm [26].

Liposome binding was first monitored on an Infinite M1000 microplate reader from Tecan Systems Inc. (San Jose, CA), with Ex/Em of 413/510nm. Cell monolayers grown on 96 well culture plates were treated with liposomes (concentrations of 250, 125, 62.5, 31.3 and 15.6 μg/ml) in 100 μl media with LPP concentrations of 2.5, 1.25, 0.63, 0.31, 0.16 or 0 mol% within the liposomes. After incubation for 30 min at 37°C in 5% CO_2, the media was removed and cells were gently rinsed twice with DPBS before fluorescence was quantified with the plate reader.

Liposome internalization and subsequent pH change were studied with both a microplate reader (quantification only) and fluorescence microscopy (imaging and quantification). Cells were plated on 35-mm petri dishes and exposed to liposomes at 50 μg/ml (64 μM) in 1.5 ml of media for 30 min at 37°C in 5% CO_2. After incubation, media was removed, cells were gently rinsed twice with DPBS, replenished with fresh media and placed back into the incubator until the indicated time point. For the quantitative study, the cells then were washed again with DPBS, treated with TrypLE Express, spun washed twice, and then the fluorescence at 510 nm was read in 100 μl of PBS on a microplate reader with dual excitations at 413 nm (pH insensitive) and 450 nm (pH sensitive). The change in the pH environment of the HPTS was monitored by taking the ratio of excitations at 450 nm/413 nm. TrypLE Express supernatant fluorescence was also measured to quantify liposomes associated with cells but not internalized. For studies combining imaging and quantification, the cells were washed with DPBS and imaged using an inverted Olympus IX71 microscope (Melville, NY) with a Carl Zeiss Achroplan 63X, NA 1.0 water immersion objective (Thornwood, NY), using two band pass excitation filters (400–420 nm (pH insensitive, Ex violet)) and (440–460 nm (pH sensitive, Ex blue)) and a single 500 nm long pass emission filter. The microscope was interfaced with a Dage-MTI CCD-300 video camera (Michigan City, IN). One phase contrast and two fluorescence images were acquired sequentially within 250 milliseconds using a software controlled filter selector. All images were analyzed using ImageJ (http://rsbweb.nih.gov/ij/). To quantify liposomal pH changes, 8 bit ratio images were created by dividing the (Ex 440–460 nm) image by the corresponding (Ex 400–420 nm) image pixel by pixel. ROIs for liposomes were created on the pH independent fluorescence images using a particle analysis plugin offered through ImageJ, then transferred to the ratio images and analyzed.

2.2.2. Binding and internalization of liposomes confirmed with MRI by loading gadolinium—T1 measurements were acquired with a 7 T imaging BioSpec system from Bruker Corporation (Billerica, MA). The magnet was equipped with a 119 mm internal

diameter gradient system from Magnex Scientific Inc. (Yarnton, Oxford, UK) which is capable of a 95 mT/m maximum gradient amplitude. PPC-1 cells, grown to 70–75% confluency in 75 cm^2 flasks, were treated for 24 hr with 20 μg/ml of Prohance-loaded liposomes containing 0.63 mol% of C-LPP-, 0.63 mol% of A-LPP-or non-targeted (NT) liposomes. Prohance is a gadolinium-based contrast agent used for magnetic resonance imaging (MRI) scans. After incubation, the media was removed and cells were gently rinsed twice with DPBS then detached using TrypLE Express. The detached cells were centrifuged at 100g for 5 min, and the supernatant was aspirated from the cells. Loosely-packed cells in a 500 μl plastic tube were placed in a high resolution, 20 mm I.D., 1H saddle probe, which was then tuned and matched to its optimum and used for radiofrequency transmission and reception. Data acquisition was accomplished with ParaVision 3 software from Bruker Corporation (Billerica, MA).

2.2.3. Cytotoxicity study—3-(4,5-Dimethylthiazol-2-yl)-2,5-diphenyltetrazolum bromide (MTT) was purchased from Invitrogen (Carlsbad, CA). The cytotoxicity of various formulations of liposomal Dox was determined by an MTT assay as described previously [27]. Cell monolayers were grown on 96-well tissue culture plates at 5,000 cells per well 24 hr prior to liposome addition. The culture medium was replaced with media containing serial dilutions of various drug formulations, including free Dox, non-targeted liposomal Dox, C-LPP-liposomal Dox and A-LPP-liposomal Dox. Following 72 hr incubation at 37°C, the cells were washed twice with DPBS and fresh media with 10 μl MTT stock solution (10 mg/ml) was added to each well. The plate was then incubated for 3 hr at 37°C. Media was then removed and dimethyl sulfoxide (100 μl) was added to dissolve the blue formazan crystals converted from MTT by live cells. Cell viability was assessed by the absorbance at 570 nm.

2.3. *In vivo* studies

All animal studies were conducted under a protocol approved by the University of California, Davis Animal Care and Use Committee. Female FVB mice, 6 weeks old, 15–25 g, were purchased from Charles River Laboratory International Inc. (Wilmington, MA).

The liposomal *in vivo* stability was validated by optical imaging of healthy mice. Mice were anesthetized with isofluorane, intravenously injected with SIDA-loaded liposomes (10 mg lipid/kg body weight), and scanned at various time points (0hr, 1hr, 6hr, 12hr, and 24hr) on the Maestro Hyperspectral Imaging System from Cambridge Research and Instrumentation, Inc. (Woburn, MA). At 24 hr, animals were euthanized, the SIDA concentration in blood was quantified *ex vivo*, and blood was further treated with 1% Triton-X 100 and heated to 50°C for 5 min to ensure that SIDA was in an unquenched state.

Liposomal binding to the tumor vasculature was confirmed by *ex vivo* imaging using Alexa 555 loaded liposomes. Mice with unilateral neu deletion mutant (NDL) tumors (2–3 mm) were anesthetized with isofluorane and intravenously injected with Alexa 555 loaded liposomes (30 mg lipid/kg body weight) or saline (n=3 each for saline, C-LPP, or NT liposomes) [28]. The NDL model was chosen for the *in vivo* studies as it is a syngeneic tumor that is similar to human HER 2+ tumors and NRP was found to be present on the

vascular surface [28]. At 24 hr, animals were injected with fluorescein-labeled Lycopersicon Esculentum (Tomato) Lectin (VectorLab, CA) (50 μg each mouse) to label the endothelium [29]. Fifteen minutes later, the animals were perfused with saline followed with 1% paraformaldehyde (Ted Pella, Inc., Redding, CA) in PBS, and the tumors were harvested and imaged using confocal microscopy. A custom-designed confocal microscope, based on a Zeiss AxioObserver equipped with a Yokogawa spinning disk confocal system and a CoolSnap HQ II CCD camera with two solid-state lasers (488 and 561 nm) was used. The microscope system was controlled by Slidebook software (Intelligent Imaging Innovations). The images were acquired with a 40× intravital lens (Objective LD C-Apochromat 40×/1.1 W Corr M27, from Carl Zeiss Microscopy, LLC, United States), with an exposure time of 10,000 and 1000 ms for 488 and 561 nm wavelengths, respectively. A glass bottom culture dish (diameter: 35mm; thickness: No.1.5) (Mat Tek Corporation, MA) was used to position the tumor on the microscope stage. Image quantification was performed with ImageJ. Squares of 4.14×10^{-5} cm^2 at the image center were cropped from the original images and analyzed to avoid the influence from the uneven distribution of the light, and ROIs for the tumor vessel were drawn on the 488nm image (Lectin) and transferred to the 561nm (Alexa 555) image. For each tumor, 3 images were analyzed.

For the therapeutic study, mice underwent unilateral transplantation of NDL tumor cells from donor mice [28], one mm^3 pieces of donor NDL tumor were transplanted into the 4^{th} mammary fat pads of 3-week-old mice. Mice were treated with liposomes when transplanted tumors reached 2–3 mm in longitudinal diameter. Efficacy studies involved 12 mice that were randomized between 3 groups (saline only, 0.63% C-LPP-Dox liposomal formulations and NT Dox liposomal formulation). NT and 0.63% C-LPP Dox liposomal formulation were manually injected over 5 seconds at a drug concentration of 6 mg Dox per kg body weight twice per week over 4 weeks. Tumor progression/regression was monitored using a Acuson Sequoia 512 ultrasound imaging system from Siemens Medical Solution USA, Inc. (Issaquah, WA) equipped with a 15L8-linear array transducer. After the region surrounding the tumor was shaved, the tumor was viewed in both the transverse and sagittal planes and the tumor boundary was fitted with an ellipse in each view measuring D_1 or D_3 and the depth D_2 is the average of depth measured in each transverse and sagittal view. Tumor volume was then calculated using the equation: $V=\pi/6\cdot(D_1\times D_2\times D_3)$. Tissues were fixed in 4% paraformaldehyde, embedded in paraffin, sectioned at 5 μm and stained with hematoxylin and eosin. Immunostaining was performed according to standard protocols.

The availability of the tumor vasculature NRP during the treatment procedure was studied by injecting NRP-targeted microbubbles and monitoring the binding with ultrasound (US), similar to[30, 31]. Briefly, microbubbles with 1,2-distearoyl-sn-glycero-3-phosphocholine (DSPC, Avanti Polar Lipids, Alabaster, AL), DSPE-PEG2k, and C-LPP (DSPC:DSPE-PEG2k:C-LPP = 90:9:1, mol:mol:mol) were made with a standard protocol, and IV injected into mice with a dose of $5–8\times10^7$ bubbles per mouse in a bolus, and three 10-sec clips were collected at 30 sec, 5 min 45 sec, and 6 min 15 sec post injection. Microbubble destruction (MBD) was performed at 6 min post injection. The US images and clips were processed with MATLAB.

2.4. Statistics

Data points represent the average of a minimum of triplicate measurements and the error bars are the standard deviations of these measurements. For individual statistical comparisons between groups, two-tailed Student's t-tests were performed to compare the means of the measured parameters. The Bonferroni correction was performed for multiple comparisons to maintain the global p value at 0.05; all values lower than 0.05 were considered significant. In addition, linear regression was performed on data sets to characterize apparent trends in data. Our optical assessment of tumors demonstrates a 10% standard deviation. Therefore, n=4 was chosen to detect a 20% change between groups for two-sided tests with alpha of 0.05 at a power of 0.8.

3. Results

3.1. Binding and internalization of targeted liposomes are influenced by ligand density and peptide terminus

NRP expression was 9.1 times higher in NRP-positive (PPC-1) as compared with NRP-negative (PC-3) cell lines (Sup. Figure 1). Binding of C-LPP liposomes and A-LPP liposomes was assessed as a function of ligand density, liposome concentration and cell line. C-LPP liposomes bound to NRP-positive cells with a peptide concentration as low as 0.16 mol% and binding was saturated with a liposomal concentration equal to or greater than 250 μg/ml (Figure 1A). C-LPP liposomes bound to PPC-1 cells at a higher density than PC-3 cells regardless of the peptide or liposome concentration (Figure 1A,B).

Punctate fluorescence was observed when C-LPP liposomes were incubated with PPC-1 cells (Sup. Figure 3). The 0.63 mol% C-LPP-liposomal formulation has a high specificity for PPC-1 (NRP+) cells, binding 83-fold more than the A-LPP-equivalent liposomal formulation at the 31 μg/ml liposome concentration (Figure 1A, C). For this reason 0.63 mol % C-LPP liposomes were chosen for all subsequent *in vivo* experiments.

The A-LPP-liposomal formulations exhibited non-specific binding. Binding of A-LPP-liposomal formulations did not saturate at the highest peptide concentrations tested and increased linearly with the concentration of liposomes regardless of NRP expression (Figure 1C and D, R^2=0.99 and R^2=0.97, respectively). A-LPP-liposomal formulations also bound to cell-free surfaces of the plate increasing the apparent accumulation (Sup. Figure 3).

3.2. HPTS facilitates detection of the pH environment

HPTS facilitates tracking of liposome internalization and trafficking as a result of changes in fluorescence intensity with the environmental pH. As the liposome moves between the endosomal and lysosomal compartments, the change in pH alters the fluorescence emissions. HPTS fluorescence emission intensity contains two complementary pH dependent peaks with excitation at 403 nm and 450 nm, as well as an isosbestic point corresponding to excitation 413 nm (Figure 2A). The ratio of fluorescence intensity following excitation at 450 nm and 413 nm was linear in the physiologic pH range of 5.75 to 7.50 (Sup. Figure 4B, R^2=0.994). Below pH 5.75 the fluorescence intensity following excitation at 450 nm was no longer linear with pH. The pH dependence of the fluorescence of HPTS did not change

when the dye was encapsulated and HPTS was impermeant to liposomes as a result of its high charge.

Endocytosis of HPTS-containing liposomes was monitored by dual fluorescence excitation using excitation light with a wavelength of 400–420 nm (pH insensitive, λEX violet) or 440–460 nm (pH sensitive, λEX blue) and with a single 500 nm emission filter (λEM) (Sup. Figure 4A). The validation of our use of this dye to monitor endocytosis is shown in Sup. Figure 4A where phase contrast and multi-wavelength images of each cell plate were first acquired. The fluorescence intensity in the violet wavelengths was used to detect the particles and the ratio of the two wavelengths in these detected regions was calculated within these ROIs. The ratio of the fluorescence at 450 and 413 nm was then calculated for the microscope and plate reader and shown to have a linear dependence on the pH of the solution (Sup. Figure 4B). When ratio images (λEX blue/λEX violet) of PPC-1 cells treated with C-LPP liposomes were viewed over 24 hr, liposomes were visible as punctate fluorescence sources gradually changing from bright to dark as endosomal acidification occurs (Sup. Figure 4C). The fluorescence ratio changed from 1.1 to 0.8 over 24 hr for PPC-1 cell monolayers treated with C-LPP liposomes, with 73% of the total change occurring within the first 6 hr (Figure 2B).

Cell pellet fluorescence measured over 24 hr using a microplate reader also demonstrated a gradual reduction in the pH environment of the HPTS. The pH fell to ~pH 6.25 in a linear fashion, similar to the gradual decline observed using fluorescence microscopy (Figure 2B).

To determine the time required for surface-bound liposomes to be internalized by cells, we analyzed the TrypLE Express supernatant following cell pelleting through centrifugation. Immediately following the liposome treatment and cell pelleting, a significant fraction of the cell-associated liposomes on the cell surface was removed by TrypLE Express. By 3 hr, 80% of the liposomes could no longer be removed by TrypLE Express and following 6 hr incubation >95% of liposomes remained associated with the cell pellet after TrypLE Express treatment (Sup. Figure 5).

Binding and internalization were then evaluated in a cell pellet, eliminating the signal from non-specific liposomal binding on cell monolayers (Figure 3). A 72-fold increase in binding of C-LPP liposomes to PPC-1 cells as compared to A-LPP liposomes was observed at 0.63 mol% LPP (Figure 3A). A-LPP liposomes were observed to bind to either NRP-positive or negative cell lines with the highest ligand concentration (Figure 3A, B). PPC-1 cells treated with C-LPP liposomes demonstrated the largest decrease in pH as compared to A-LPP liposomes, dropping a full pH unit for the formulations containing the lowest peptide percentages (Figure 3C). C-LPP liposomes bound to a small extent to PC-3 cells (Figure 3B) and a decrease in pH, as compared to A-LPP liposomes, was observed for all peptide concentrations (Figure 3D). NT and A-LPP liposomes do not demonstrate a decrease in pH below 6.74 suggesting that they do not enter the same endosomal environment as C-LPP liposomes.

3.3. Enhanced internalization of C-LPP liposomes containing an MRI contrast agent

We also verified that the enhanced internalization of C-LPP liposomes could be detected by MRI by incubating Gd-loaded liposomes with the NRP+ cells. Control cells not treated with liposomal gadolinium contrast agents had the longest T1 value (2250 ms), which is in the expected range for a cell pellet (Figure 4). C-LPP-liposomal gadolinium reduced the T1 by 21% to 1765 ms in comparison to a 7.6% reduction with A-LPP-liposomal gadolinium (Figure 4).

3.4. Enhanced therapeutic efficacy of C-LPP liposomes *in vitro*

For LPP concentrations above 0.63 mol%, Dox loading increased with decreasing LPP content. For lower peptide concentrations, ~100% loading efficiency was achieved for all subsequent formulations (Sup. Figure 6A). Loading efficiencies of ~70% were observed when loading 2.5 mol% LPP liposomes for both carboxyl and amide formulations.

The intraliposomal Dox was present in an aggregated state for both non-targeted and LPP-targeted liposomes as shown by the red shift in the excitation peak and the loss of the 650 nm shoulder (Sup. Figure 6B). Therefore, the presence of LPP in the liposome bilayer does not alter the ammonium sulfate loading of Dox.

A subset of the resulting C-LPP-conjugated, Dox-loaded liposomal formulations increased the efficacy against PPC-1 cells, as compared with NT particles. When evaluated with the PPC-1 cell line, the cytotoxicity of the C-LPP-Dox-containing liposomes with a LPP concentration greater than 0.63 mol% had an IC50 below 1.34 μM, while formulations with less than 0.31 mol% LPP had no increase in cytotoxicity as compared to NT-liposomes (Figure 5A). A-LPP liposomes were only effective with the highest concentration of LPP, where formulations containing less than 2.5 mol% were similar in efficacy to NT liposomes (Figure 5B). At 0.63 mol% LPP, C-LPP containing formulations were 6.15-fold more cytotoxic to PPC-1 cells than A-LPP containing formulations at 5.3 μM Dox (Figure 5C). In PC-3 cells, neither C-LPP nor A-LPP liposomes increased efficacy as compared to NT control liposomes (Sup. Figure 7).

3.5. Enhanced therapeutic efficacy of C-LPP liposomes *in vivo*

Both C-LPP-and NT liposomes circulated stably and a gradual increase in fluorescence was observed over 24 hr, increasing 4.1× and 2.6× in fluorescence intensity, respectively (Sup. Figure 8A–B). Optical images of FVB mice treated with NT and 0.63 mol% C-LPP liposomes from a typical experiment demonstrated increasing fluorescence as the fluorescence quenching was reduced. An ROI was placed on the back of the mice as an indicator for liposomal stability and the fluorescence intensity was tracked over 24 hr (Sup. Figure 8B). The addition of 0.63 mol% targeting ligand, C-LPP, to the surface of the liposome had no significant effect on the *in vivo* circulation as compared to the NT formulation (0 mol% C-LPP). Blood fluorescence was similar between the targeted and non-targeted formulations in mice injected with liposomes loaded with either SIDA or Dox at 24 hr after injection (Figure 6A).

The accumulation of both C-LPP-and NT liposomes *in vivo* was evaluated using Alexa 555 as a liposomal cargo and assessed with confocal microscopy (Figure 6B–C). In this scenario, for untreated tumors, the fluorescence intensity was higher in tumors treated with either C-LPP- or NT liposomes than those treated with saline. Further, the tumor fluorescence intensity was higher in mice injected with C-LPP liposomes as compared with NT liposomes, and punctate accumulation of Alexa 555 was co-localized with blood vessels in tumors treated with C-LPP liposomes. We found that the accumulation of the C-LPP liposomes was reduced as compared with the NT liposomes after the 4-week course of treatment as measured through ex vivo optical imaging of the tumors (Figure 6D).

As a result of the differences between the accumulation of fluorophore-loaded and doxorubicin-loaded liposomes, and the observation that a substantial fraction of the C-LPP liposomes initially bound to the vascular surface, we sought to evaluate the density of the NRP ligand on the endothelial surface with ultrasound molecular imaging (Figure 7). We found that the accumulation of the C-LPP microbubbles on the tumor vasculature was lower following treatment and that this decrease occurred with either targeted or non-targeted liposomal doxorubicin therapy (Figure 7B).

The toxicity and efficacy of the liposomal formulations was then assessed. Mice bearing unilateral NDL tumors were treated with NT or C-LPP liposomes for 28 days at a Dox concentration of 6 mg/kg twice per week. Dox fluorescence in the heart was 2.3-fold higher in NT liposomal Dox-treated mice when compared to the C-LPP-liposomal Dox formulation (Figure 8A). Maestro images of Dox fluorescence confirmed skin toxicities were correlated with Dox accumulation (Figure 8B). Dox toxicity was also observed through the weight change of the mice during the final week of the study, with the NT liposomal Dox treatment group losing 10% of their body weight in comparison to the 2% loss in weight for the C-LPP-liposomal Dox group (Figure 8C). Cardiac hypertrophy was also assessed as an indicator of cardio-toxicity. Heart weight did not increase in the NT and C-LPP-groups, as compared to the saline control group (Figure 8D).

The therapeutic efficacy of the 0.63 mol% targeted liposomes was confirmed *in vitro* as well as *in vivo*. At Dox concentrations of 10 μM and higher, C-LPP liposomes have greater efficacy as compared to the NT liposome and 95% cell death occurred at concentrations above 30 μM Dox (Figure 8E). Groups treated with NT and C-LPP-liposomal Dox had a cessation of tumor growth over 28 days with average tumor volumes at the final time point of 0.01 and 0.007 cm^3, respectively (Figure 8F). The control group receiving saline injections was sacrificed at day 17 as the average tumor volume exceeded 0.5 cm^3 (Figure 8F). Tumors were also weighed after mice were sacrificed confirming ultrasound measurements that the C-LPP-liposome treated tumors were slightly smaller than the NT tumors (27.2 mg and 49.9 mg, respectively) (Figure 8D). Tissue was stained with hematoxylin and eosin to better visualize the tissue morphology. Both NT and C-LPP-liposomal Dox treated groups had enlarged nuclei and disordered cell morphologies (Sup. Figure 9). Saline control tumor cells were well ordered and nuclei were not enlarged.

4. Discussion

We incorporated an NRP lipo-PEG-peptid (LPP) into long-circulating liposomes to increase the therapeutic index of encapsulated Dox. We chose to use the short linear peptide CRPPR as a ligand, comparing the results for a C-terminal carboxyl-terminated peptide with those of a C-terminal amide-terminated peptide. The resulting C-LPP liposomes bound to the NRP-positive PPC-1 cells but did not bind to the NRP-negative PC-3 cell line. Binding was observed with peptide concentrations as low as 0.16 mol%, facilitating the design of a long circulating, yet effective particle. Our results differ from technology using iRGD to deliver therapeutics into the extravascular tumor parenchyma as a multistep mechanism is not required for effective NRP targeting [9, 32]. The multivalent targeting of our liposomal constructs allow for high affinity targeting to NRP, where previous studies required RGD binding to α_v integrins for initial tumor accumulation. The ability to specifically target NRP receptors with low mol% LPP in long circulating vehicles distinguishes our results from previously described tumor-targeting peptides [33]. Further, we choose to evaluate the accumulation and efficacy of the targeted therapeutic over the course of a 4-week, twice per week therapy as compared with a non-targeted liposomal therapy.

4.1 Binding and internalization

Using *in vitro* cellular assays and *in vivo* optical imaging, a C-LPP-liposomal Dox particle was engineered to have an improved therapeutic index. In a monolayer culture, binding of the C-LPP liposomes was 83-fold greater than control liposomes and was receptor-limited, with saturation observed at high liposome concentrations. The identical peptide sequence bearing an amide terminus did not bind specifically, accumulating only with a high peptide concentration and adhering equally to NRP positive and negative cell lines. For C-LPP liposomes, the overall charge was +1 with the terminal arginine residue being a zwitterion (thus uncharged). The CRPPR-LPP with a C-terminal amide (A-LPP) increased the overall positive charge from +1 to +2 with the terminal arginine residue containing a positive charge. C-LPP-liposome binding was mediated through a protease-sensitive cell-surface receptor, in our case hypothesized to be NRP, with the majority of bound liposomes being internalized within 3 hr of binding. C-LPP-liposome binding differed between two cell lines as a function of the NRP expression levels. Binding of C-LPP liposomes was greater for NRP-positive, as compared with the NRP-negative cell line, where the difference in NRP expression level was 9.1-fold.

Measuring the change in HPTS fluorescence following cellular binding allowed us to monitor cellular internalization kinetics by using fluorescence microscopy in combination with image processing. Within 6 hr, 73% of C-LPP liposomes were in acidic environments. Liposomes are subjected to increasing acidification along the endosomal pathway from early endosomes to lysosomes, which is used here as an indicator of cellular internalization. A-LPP liposomes that bound non-specifically to cells did not experience a decrease in pH following cell association as they remained surface bound and were not internalized by the cells. Using 0.63 mol% C-LPP liposomes, superior binding and internalization was also observed by MRI imaging of T1 times as compared to A-LPP-particles, demonstrating the

feasibility of using an MRI contrast agent to monitor liposome internalization in an *in vivo* imaging study.

Liposomes were successfully loaded with Dox using an ammonium sulfate gradient. No differences in loading were observed between C-LPP and A-LPP liposomes, both loading at ~100% when the LPP concentration was below 0.63 mol%. It is hypothesized that the LPP reduces the aqueous internal volume, and when incorporated at sufficiently high levels it hinders Dox loading. C-LPP and A-LPP differ in size by only a single Dalton and the loading efficiencies remain nearly identical as a function of LPP mol%, regardless of the peptide terminus. The ammonium sulfate gradient approach is useful as it does not require the liposomes to be prepared in an acidic pH and the stability of the drug in the liposome is greater due to the aggregation and gelation of the anthracycline sulfate salt which occurred in all of our liposomal formulations.

These LPP-targeted liposomal Dox particles were then applied in an *in vitro* cellular efficacy study. Cell toxicity trends followed results observed with imaging with one noteworthy difference. While all peptide concentrations of C-LPP liposomes bound to PPC-1 cells, as determined through HPTS fluorescence, only those with 0.63 mol% or greater peptide concentration exhibited increased cytotoxicity as compared to a NT liposome control. We hypothesize that a C-LPP threshold concentration is required for endosomal escape. Alternatively, C-LPP may have a combined synergistic effect with Dox and therefore a threshold concentration of C-LPP is needed.

4.2 Stability in circulation and tumor accumulation

Using the most promising LPP-targeted liposomal particle from the *in vitro* studies, we evaluated the efficacy of 0.63 mol% C-LPP liposomes. Using the *in vivo* optical imaging technique described previously [21], we loaded the particle with a quenched near-infrared (NIR) fluorophore and demonstrated that the circulation was equivalent to a NT liposome control. Similarly, 24 hr after injection of Dox-loaded particles, the circulating Dox concentration was identical for both NT and C-LPP liposomes. This demonstrates an encouraging pharmacokinetic profile in that the circulation of the targeted liposome was approximately equivalent to the NT control. Optical imaging to detect dequenching of an NIR fluorophore is a very sensitive and robust method to detect liposomal destruction and clearance from the blood pool and therefore would be expected to detect differences. To validate *in vivo* optical imaging measurements, mouse blood was collected at 24 hr and blood fluorescence intensity was similar for both formulations, confirming the *in vivo* imaging results.

Accumulation of the C-LPP liposomes was then assessed in a tumor model. We found that while the C-LPP liposomes loaded with a NIR fluorophore accumulated significantly more than the non-targeted control, this enhanced accumulation was not observed with doxorubicin-loaded liposomes after 4 weeks of C-LPP Dox liposome treatment. Instead, at this time point, the accumulation of the non-targeted control exceeded that of the targeted liposome. One mechanism for this change in accumulation may be a reduction in the vascular surface receptor for CRPPR over the course of treatment.

4.3 Therapeutic efficacy and toxicity

The treatment of highly aggressive syngeneic NDL tumors, with doubling times of a few days, requires aggressive treatment regimes in mice. In this study, the volume of saline-treated tumors exceeded 580 mm^3 within 17days. Dox-loaded liposomes were injected bi-weekly over 4 weeks and successfully produced tumor regression. Further, C-LPP liposomes were effective in halting tumor growth while also minimizing skin damage and cardiotoxicity. Reducing the toxicity of such liposomal formulations remains important. NT liposomal Dox accumulates in the skin of mice that have been prepared for ultrasound imaging, while the C-LPP-liposomal Dox particles did not accumulate. Such toxicities are common to patients treated with the commercial liposomal Dox formulation (Doxil), with intense pain in the hands and feet known as the Hand-Foot Syndrome (HFS) or Palmar-Plantar Erythrodysesthesia (PPE) [34, 35]. The reduction in skin toxicity with the C-LPP liposomes is assumed to result from reduced extravasation and vascular targeting in normal tissue due to increased liposome size, steric effects and particle charge.

The therapeutic study was ended at 29 days due to the relatively high toxicity of the NT-liposomal formulation, demonstrated by dramatic weight loss and skin toxicity. Dox accumulation was lower in the hearts of mice treated with the targeted liposomes, as compared with the NT formulation. However, the heart weight, which is an indicator of toxicity, was not significantly different between the groups. Future *in vivo* experiments treating with a lower dose of liposomal Dox will be required to determine the minimal drug concentrations required for efficacious treatment and assess differences in efficacy with lower Dox dosage.

Our results also suggest the importance of longitudinal assessment of receptor density for targeted therapies. Molecular imaging techniques provide the opportunity to ensure that the targeted therapeutic will continue to accumulate over repeated treatments or with other changes in receptor expression (e.g. with changes in angiogenic vessel density).

In summary, C-LPP liposomes with a low (0.63 mol%) concentration of the CRPPR peptide demonstrated extended blood circulation. We confirmed the substantial differences in targeting and internalization between amide- and carboxyl-terminated RXXR peptides. While both non-targeted and C-LPP liposomes accumulated in tumors, the C-LPP liposomes preferentially co-localized with tumor blood vessels prior to the initiation of therapy. However, changes in receptor density reduced accumulation over the course of therapy. The C-LPP-liposomal Dox formulation was tested in NDL-tumor bearing mice and resulted in cessation of tumor growth and a reduction in Dox toxicity as compared to a non-targeted liposomal Dox formulation. Based on these results, C-LPP-liposomal Dox merits further evaluation as an antineoplastic therapy and ultrasound molecular imaging may provide a suitable means to assess receptor density prior to and during treatment.

Supplementary Material

Refer to Web version on PubMed Central for supplementary material.

Acknowledgments

The authors acknowledge the support of NIHR01CA134549, NIHR01CA112356, NIHR01CA103828, T32EB003827 and the National Heart Lung and Blood Institute of the NIH as a Program of Excellence in Nanotechnology award (HHSN268201000043C). The authors appreciate the assistance of Dr. Sochiro Yamada in confocal imaging and the Center for Molecular and Genomic Imaging. The NDL cell line was developed and provided through Dr. Jane Qian Chen, UCD Center for Comparative Medicine.

References

1. Mills JK, Needham D. Targeted drug delivery. Expert Opinion on Therapeutic Patents. 1999; 9:1499–1513.
2. Gregoriadis G, Ryman BE. Lysosomal localization of -fructofuranosidase-containing liposomes injected into rats. The Biochemical journal. 1972; 129:123–133. [PubMed: 4646772]
3. Garcia AA, Kempf RA, Rogers M, Muggia FM. A phase II study of Doxil (liposomal doxorubicin): lack of activity in poor prognosis soft tissue sarcomas. Annals of oncology : official journal of the European Society for Medical Oncology / ESMO. 1998; 9:1131–1133. [PubMed: 9834828]
4. Kong G, Anyarambhatla G, Petros WP, Braun RD, Colvin OM, Needham D, Dewhirst MW. Efficacy of liposomes and hyperthermia in a human tumor xenograft model: importance of triggered drug release. Cancer research. 2000; 60:6950–6957. [PubMed: 11156395]
5. Drummond DC, Meyer O, Hong K, Kirpotin DB, Papahadjopoulos D. Optimizing liposomes for delivery of chemotherapeutic agents to solid tumors. Pharmacological reviews. 1999; 51:691–743. [PubMed: 10581328]
6. Torchilin VP. Drug targeting. European journal of pharmaceutical sciences : official journal of the European Federation for Pharmaceutical Sciences. 2000; 11(Suppl 2):S81–S91. [PubMed: 11033430]
7. Gabizon A, Horowitz AT, Goren D, Tzemach D, Shmeeda H, Zalipsky S. In vivo fate of folate-targeted polyethylene-glycol liposomes in tumor-bearing mice. Clinical cancer research : an official journal of the American Association for Cancer Research. 2003; 9:6551–6559. [PubMed: 14695160]
8. Li WM, Mayer LD, Bally MB. Prevention of antibody-mediated elimination of ligand-targeted liposomes by using poly(ethylene glycol)-modified lipids. The Journal of pharmacology and experimental therapeutics. 2002; 300:976–983. [PubMed: 11861806]
9. Teesalu T, Sugahara KN, Kotamraju VR, Ruoslahti E. C-end rule peptides mediate neuropilin-1-dependent cell, vascular, and tissue penetration. Proceedings of the National Academy of Sciences of the United States of America. 2009; 106:16157–16162. [PubMed: 19805273]
10. Straume O, Akslen LA. Increased expression of VEGF-receptors (FLT-1, KDR, NRP-1) and thrombospondin-1 is associated with glomeruloid microvascular proliferation, an aggressive angiogenic phenotype, in malignant melanoma. Angiogenesis. 2003; 6:295–301. [PubMed: 15166498]
11. Broholm H, Laursen H. Vascular endothelial growth factor (VEGF) receptor neuropilin-1's distribution in astrocytic tumors. APMIS : acta pathologica, microbiologica, et immunologica Scandinavica. 2004; 112:257–263.
12. Stephenson JM, Banerjee S, Saxena NK, Cherian R, Banerjee SK. Neuropilin-1 is differentially expressed in myoepithelial cells and vascular smooth muscle cells in preneoplastic and neoplastic human breast: a possible marker for the progression of breast cancer. International journal of cancer. Journal international du cancer. 2002; 101:409–414. [PubMed: 12216067]
13. Fakhari M, Pullirsch D, Abraham D, Paya K, Hofbauer R, Holzfeind P, Hofmann M, Aharinejad S. Selective upregulation of vascular endothelial growth factor receptors neuropilin-1 and-2 in human neuroblastoma. Cancer. 2002; 94:258–263. [PubMed: 11815985]
14. Sugahara KN, Teesalu T, Karmali PP, Kotamraju VR, Agemy L, Greenwald DR, Ruoslahti E. Coadministration of a tumor-penetrating peptide enhances the efficacy of cancer drugs. Science. 2010; 328:1031–1035. [PubMed: 20378772]

15. Zhang H, Kusunose J, Kheirolomoom A, Seo JW, Qi J, Watson KD, Lindfors HA, Ruoslahti E, Sutcliffe JL, Ferrara KW. Dynamic imaging of arginine-rich heart-targeted vehicles in a mouse model. Biomaterials. 2008; 29:1976–1988. [PubMed: 18255141]
16. Zhang H, Li N, Sirish P, Mahakian L, Ingham E, Curry FR, Yamada S, Chiamvimonvat N, Ferrara KW. The cargo of CRPPR-conjugated liposomes crosses the intact murine cardiac endothelium. Journal of controlled release : official journal of the Controlled Release Society. 2012; 163:10–17. [PubMed: 22776291]
17. Zhang L, Hoffman JA, Ruoslahti E. Molecular profiling of heart endothelial cells. Circulation. 2005; 112:1601–1611. [PubMed: 16144998]
18. Straubinger RM, Hong K, Friend DS, Papahadjopoulos D. Endocytosis of liposomes and intracellular fate of encapsulated molecules: encounter with a low pH compartment after internalization in coated vesicles. Cell. 1983; 32:1069–1079. [PubMed: 6404557]
19. Straubinger RM, Papahadjopoulos D, Hong KL. Endocytosis and intracellular fate of liposomes using pyranine as a probe. Biochemistry. 1990; 29:4929–4939. [PubMed: 2163672]
20. Anderson C, Hu X, Tlaxca X, Haughtling R, Lawrence M, Ferrara KW, Rychak JJ. Ultrasound Molecular Imaging of Tumor Angiogenesis with a Novel αVβ3-Integrin Targeted Microbubble Contrast Agent. Investigative Radiology. 2011; 46:215–224. [PubMed: 21343825]
21. Paoli EE, Kruse DE, Seo JW, Zhang H, Kheirolomoom A, Watson KD, Chiu P, Stahlberg H, Ferrara KW. An optical and microPET assessment of thermally-sensitive liposome biodistribution in the Met-1 tumor model: Importance of formulation. Journal of controlled release : official journal of the Controlled Release Society. 2010; 143:13–22. [PubMed: 20006659]
22. Safra T, Muggia F, Jeffers S, Tsao-Wei DD, Groshen S, Lyass O, Henderson R, Berry G, Gabizon A. Pegylated liposomal doxorubicin (doxil): reduced clinical cardiotoxicity in patients reaching or exceeding cumulative doses of 500 mg/m2. Annals of oncology : official journal of the European Society for Medical Oncology / ESMO. 2000; 11:1029–1033. [PubMed: 11038041]
23. Qin S, Seo JW, Zhang H, Qi J, Curry FR, Ferrara KW. An imaging-driven model for liposomal stability and circulation. Molecular pharmaceutics. 2010; 7:12–21. [PubMed: 19621944]
24. Hope MJ, Bally MB, Webb G, Cullis PR. Production of large unilamellar vesicles by a rapid extrusion procedure: characterization of size distribution, trapped volume and ability to maintain a membrane potential. Biochimica et biophysica acta. 1985; 812:55–65. [PubMed: 23008845]
25. Lasic DD, Frederik PM, Stuart MC, Barenholz Y, McIntosh TJ. Gelation of liposome interior. A novel method for drug encapsulation. FEBS letters. 1992; 312:255–258. [PubMed: 1426260]
26. Wolfbeis OS, Furlinger E, Kroneis H, Marsoner H. Fluorimetric analysis. 1 A study on fluorescent indicators for measuring near neutral physiological pH-values. . Fresenius Zeitschrift Fur Analytische Chemie. 1983; 314:119–124.
27. Mosmann T. Rapid colorimetric assay for cellular growth and survival: application to proliferation and cytotoxicity assays. Journal of immunological methods. 1983; 65:55–63. [PubMed: 6606682]
28. Cardiff RD, Engelberg JA, Munn RJ, Miller CH, Walls JE, Chen JQ, Velásquez-García HA, Galvez JJ, Bell KJ, Beckett LA, Li YJ, Borowsky AD. Quantitation of fixative-induced morphologic and antigenic variation in mouse and human breast cancers. Laboratory Investigation. 2013; 93:480–497. [PubMed: 23399853]
29. Inai T, Mancuso M, Hashizume H, Baffert F, Haskell A, Baluk P, Hu-Lowe DD, Shalinsky DR, Thurston G, Yancopoulos GD, McDonald DM. Inhibition of vascular endothelial growth factor (VEGF) signaling in cancer causes loss of endothelial fenestrations, regression of tumor vessels, and appearance of basement membrane ghosts. Am. J. Pathol. 2004; 165:35–52. [PubMed: 15215160]
30. Borden MA, Zhang H, Gillies RJ, Dayton PA, Ferrara KW. A stimulus-responsive contrast agent for ultrasound molecular imaging. Biomaterials. 2008; 29:597–606. [PubMed: 17977595]
31. Anderson CR, Hu XW, Zhang H, Tlaxca J, Decleves AE, Houghtaling R, Sharma K, Lawrence M, Ferrara KW, Rychak JJ. Ultrasound Molecular Imaging of Tumor Angiogenesis With an Integrin Targeted Microbubble Contrast Agent. Investigative Radiology. 2011; 46:215–224. [PubMed: 21343825]

32. Alberici L, Roth L, Sugahara KN, Agemy L, Kotamraju VR, Teesalu T, Bordignon C, Traversari C, Rizzardi GP, Ruoslahti E. De novo design of a tumor-penetrating peptide. Cancer research. 2013; 73:804–812. [PubMed: 23151901]

33. Bae YH, Park K. Targeted drug delivery to tumors: myths, reality and possibility. Journal of controlled release : official journal of the Controlled Release Society. 2011; 153:198–205. [PubMed: 21663778]

34. Zuehlke RL. Erythematous eruption of the palms and soles associated with mitotane therapy. Dermatologica. 1974; 148:90–92. [PubMed: 4276191]

35. Yokomichi N, Nagasawa T, Coler-Reilly A, Suzuki H, Kubota Y, Yoshioka R, Tozawa A, Suzuki N, Yamaguchi Y. Pathogenesis of Hand-Foot Syndrome induced by PEG-modified liposomal Doxorubicin. Human cell. 2013; 26:8–18. [PubMed: 23386177]

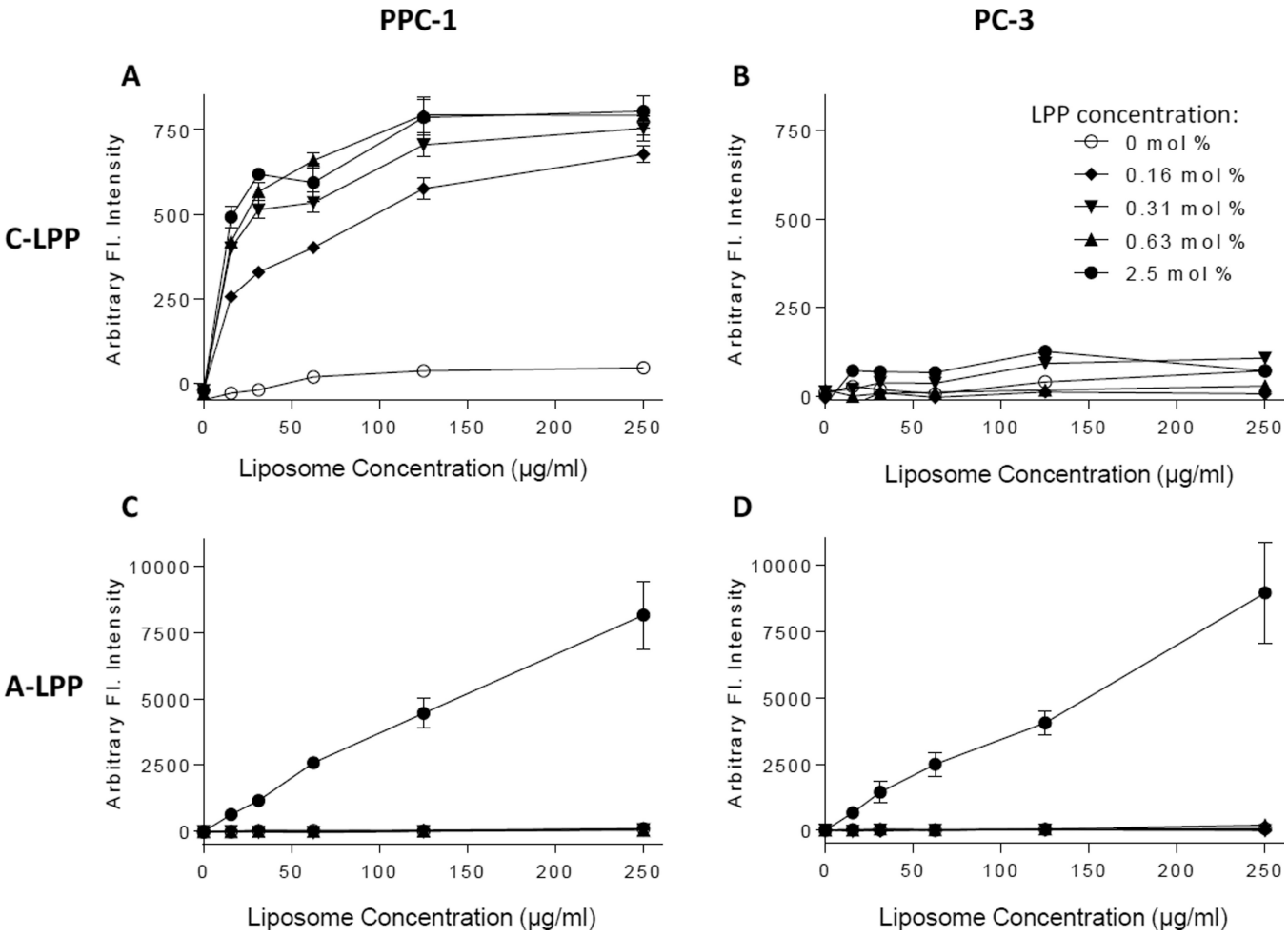

Figure 1.

HPTS fluorescence intensity (excitation-413 nm and emission-510 nm) of PPC-1 and PC-3 cell monolayers for varied liposome and peptide concentrations after 30 min incubation with liposomes followed by a PBS wash. Cell monolayers on 96 well collagen-treated plates were exposed to liposomes containing HPTS in 100 µl complete cell media, HSPC/CHOL/DSPE-PEG2k/LPP (56:39:5-X:X), X ranging from 2.5 to 0 mol%. (A) Binding of C-LPP liposomes to PPC-1 cells saturates at high lipid concentrations. Low mol% of C-LPP is sufficient for significant liposome binding to PPC-1 cells as compared to NT liposomes. (B) C-LPP liposomes do not bind to PC-3 cells at a detectable level. A-LPP-liposome binding is effective only at the highest peptide concentration for (C) PPC-1 or (D) PC-3 cells and does not saturate (indicating a non-specific interaction). An expanded view of C and D (same y range as in A and B) is shown in (Sup. Figure 2A and B, respectively).

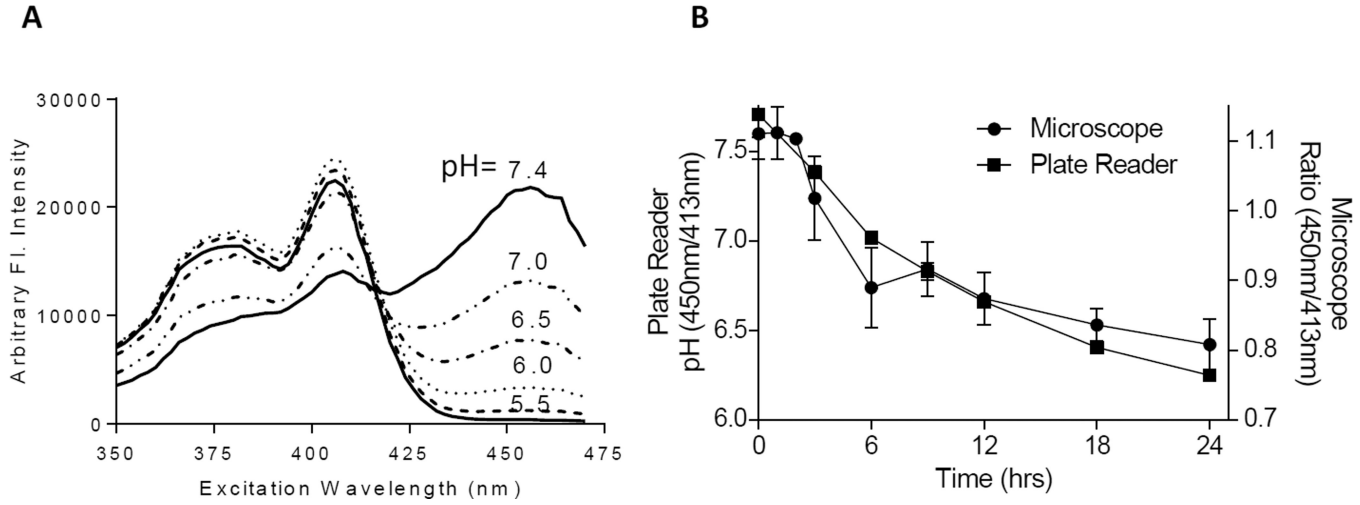

Figure 2.

HPTS fluorescent pH properties and use for tracking intracellular kinetics. (A) Excitation spectra for HPTS at pH values ranging from pH 5.5 to 7.4 while holding the emission wavelength constant at 510 nm. (B) The pH change of C-LPP liposomes over 24 hr following incubation with PPC-1 cells was similar when quantified with fluorescence microscopy or a plate reader.

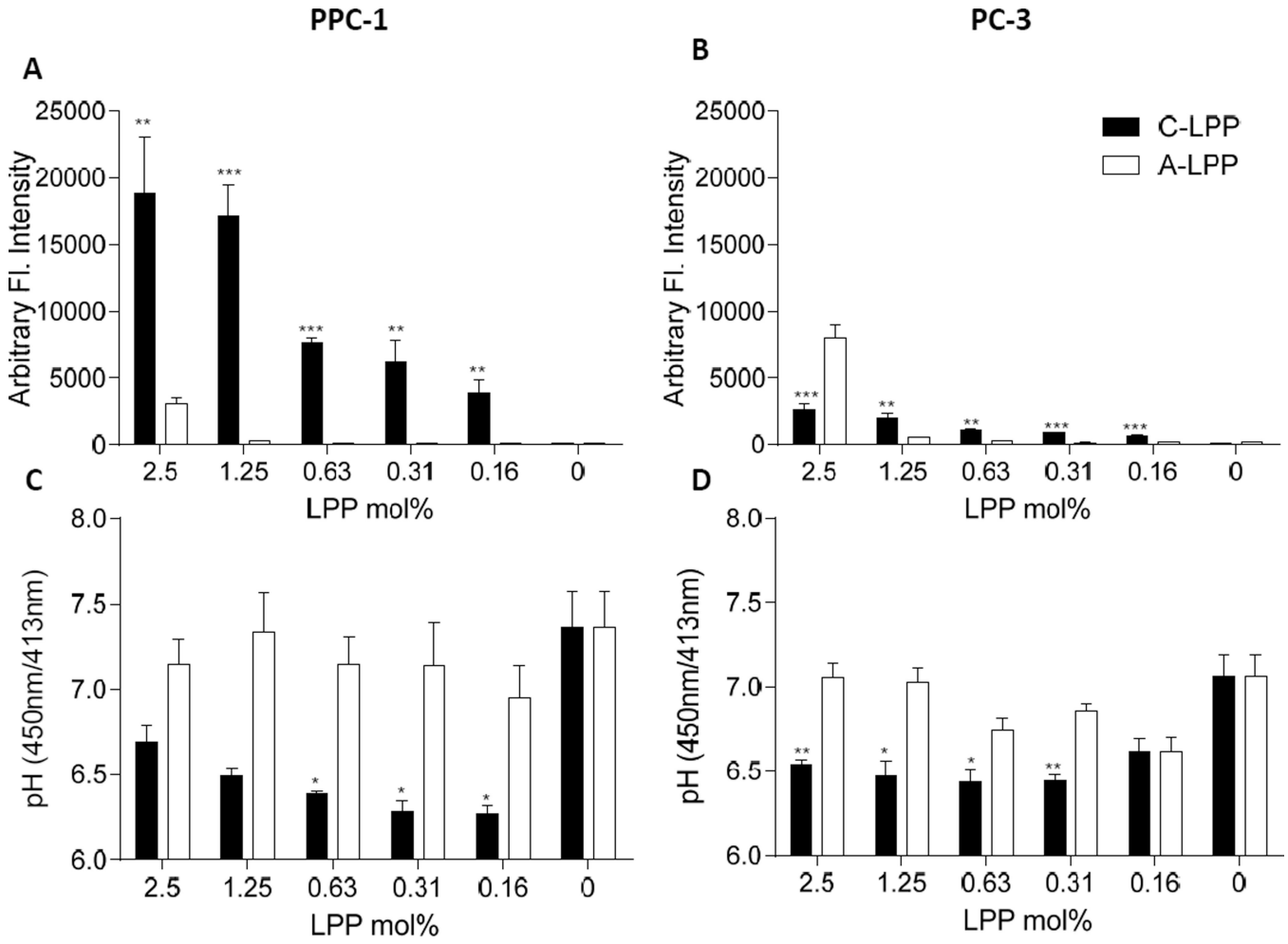

Figure 3.

HPTS fluorescence intensity and pH of cell pellet after 30 min liposome treatment followed by PBS wash and 24 hr incubation in fresh media. PPC-1 and PC-3 cell monolayers on 35-mm petri dishes were exposed to 50 μg/ml of HSPC/CHOL/DSPE-PEG2k/LPP (56:39:5-X:X) liposomes containing HPTS in 1.5 ml complete cell media, X ranging from 2.5 to 0 mol%. (A) Binding of C-LPP liposomes to PPC-1 cells was greater than A-LPP-and NT liposomes (0 mol% LPP). (B) Binding of C-LPP and A-LPP liposomes to PC-3 cells was low and observed only at the highest LPP mol%. (C-D) The change in pH environment of the HPTS was monitored by the ratio of excitations 450 nm/413 nm. Substantial differences in pH occurred for C-LPP liposomes, as compared to A-LPP targeted liposomes in both (C) PPC-1 and (D) PC-3 cells. For comparisons of C-LPP and corresponding A-LPP values. * $p<0.05$, ** $p<0.01$, *** $p<0.001$.

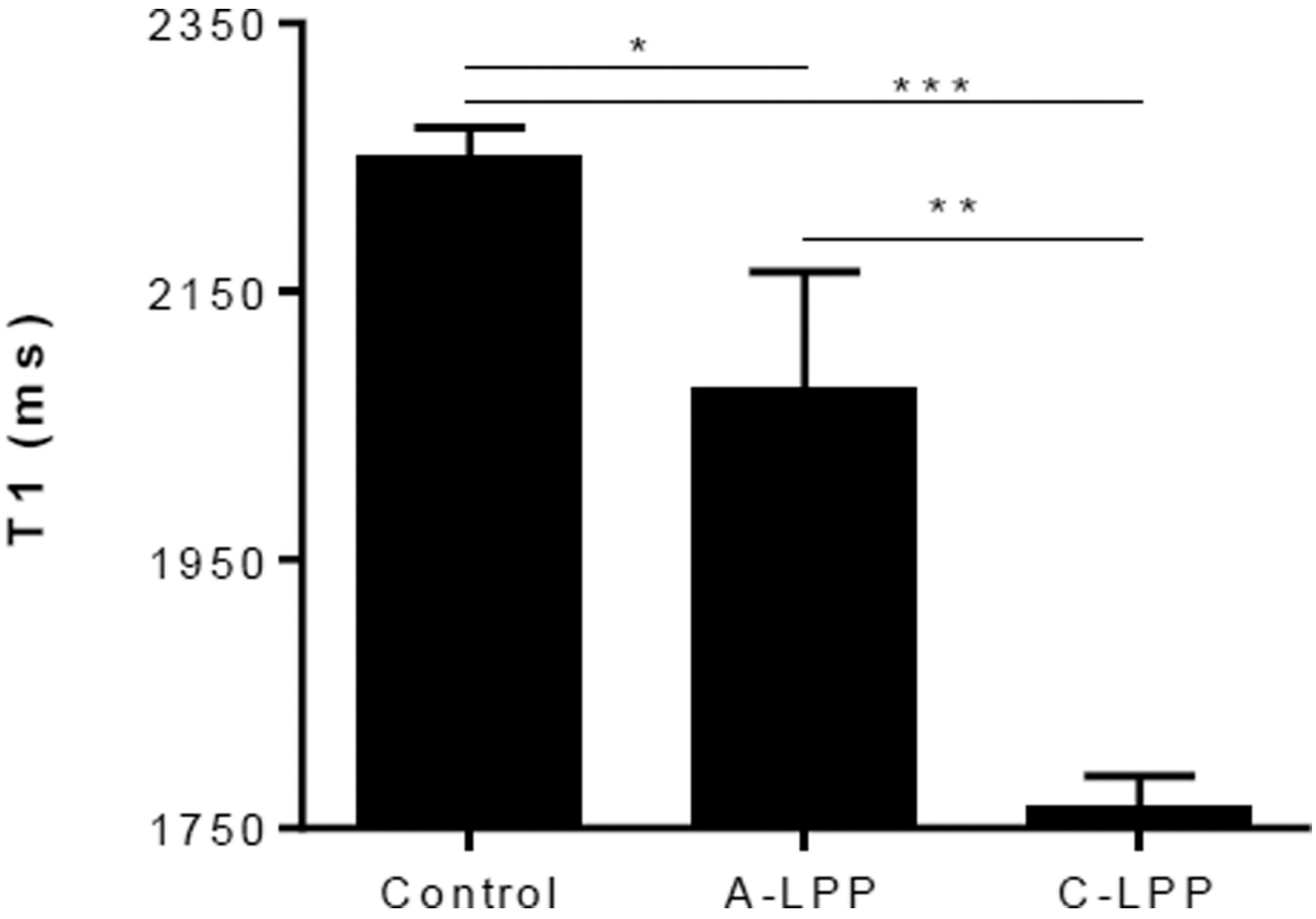

Figure 4.

The enhanced internalization of C-LPP liposomes was detected by MRI: T1 measurements were performed in a 7T imaging system (BioSpec). PPC-1 cells were treated with 0.63 mol % C-LPP or A-LPP-Prohance-loaded liposomes. The magnet was equipped with a 119 mm internal diameter gradient system (Magnex Scientific) capable of 95 mT/m maximum amplitude. Loosely packed cells in a 500 μl plastic tube were placed in a high resolution, 20 mm I.D., 1H saddle probe, which was then tuned and matched to its optimum and used for radiofrequency transmission and reception. Data acquisition was accomplished within ParaVision 3 software (Bruker BioSpin). * $p<0.05$, ** $p<0.01$, *** $p<0.001$

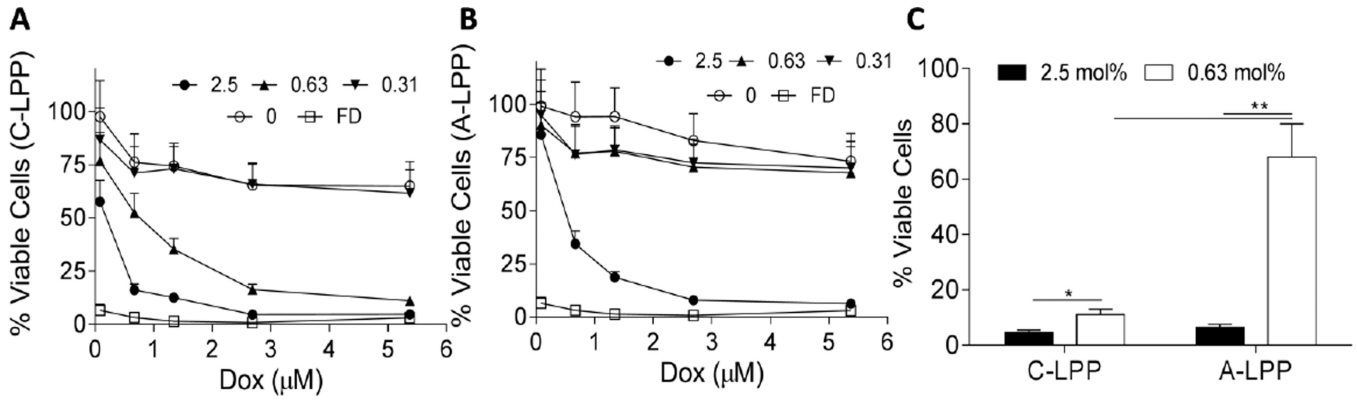

Figure 5.

MTT assay of Dox loaded targeted liposomes (2.5 – 0 mol%) and free Dox (FD) treated for 72 hr with PPC-1 cells. (A) C-LPP liposomes of 0.63 mol% or greater significantly inhibited cell growth as compared to NT liposomes (0 mol% LPP). (B) A-LPP liposomes had a significant efficacy only at 2.5 mol% LPP. (C) C-LPP and A-LPP liposomes efficacy at 5.3 μM Dox with 2.5 or 0.63 mol% LPP. * $p<0.01$, ** $p<0.001$.

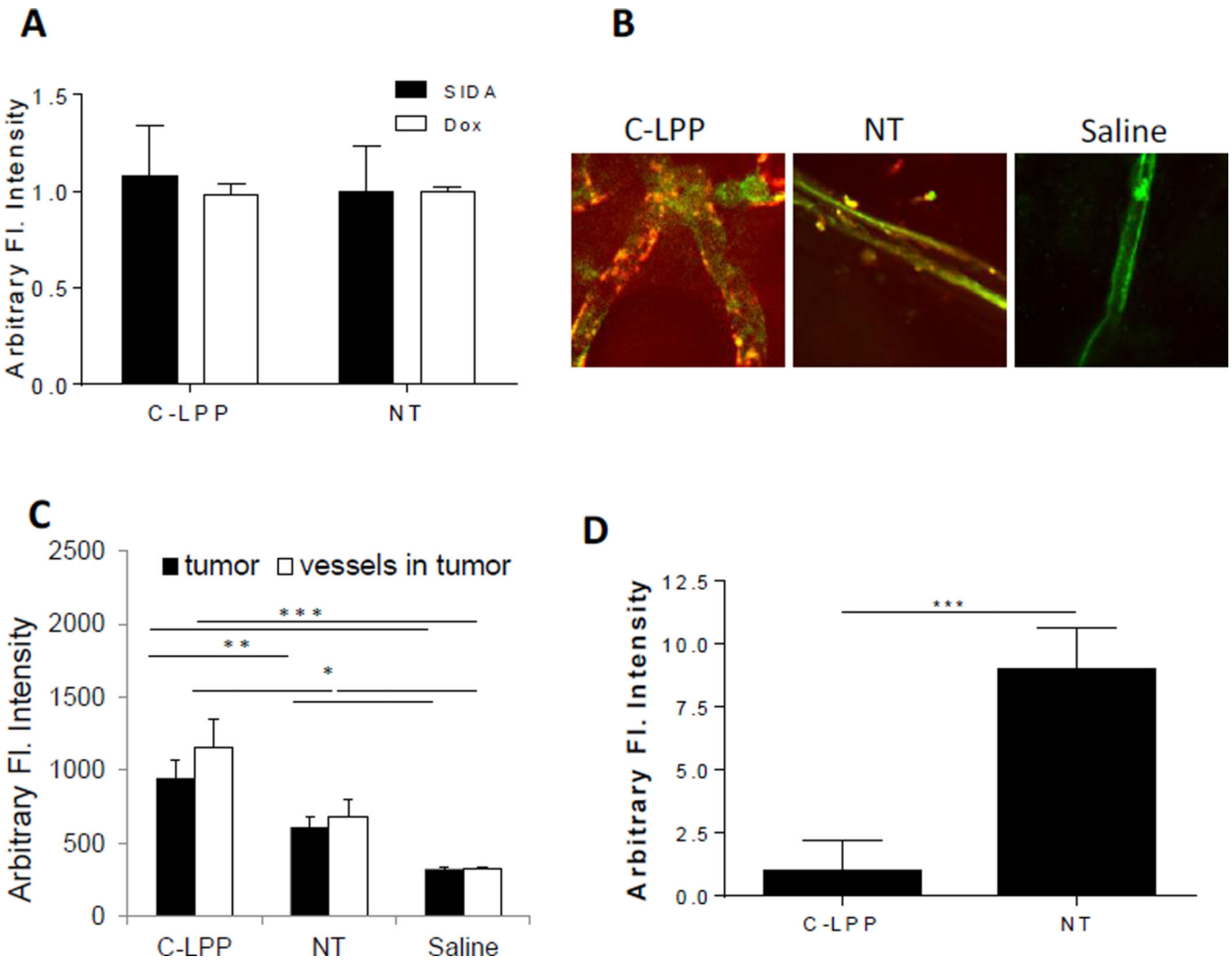

Figure 6.

Circulation and accumulation of liposomal vehicles of carboxyl-terminated NRP-targeted liposomes (C-LPP) and non-targeted (NT) control liposomes. (A) *Ex vivo* measurements for Dox and SIDA fluorescence in blood 24 hr following final liposomal injection. (B) *Ex vivo* confocal images for tumors 24 hr after injections of C-LPP liposomes (left), NT-liposomes (middle), and saline (right). Alexa 555 (red) was loaded into liposomes as a model drug, and FITC-Lectin (green) was used to localize blood vessels. (C) Quantification of the red channel (Alexa 555) for the tumor (entire field of view) and blood vessels from Figure 6B. ROIs of blood vessels were drawn on the green channel (FITC-lectin) and transferred to the red channel and analyzed. (D) *Ex vivo* measurements for Dox fluorescence in tumors 24 hr following final liposomal injection after 4 weeks of treatment. * $p<0.05$, ** $p<0.01$, *** $p<0.001$.

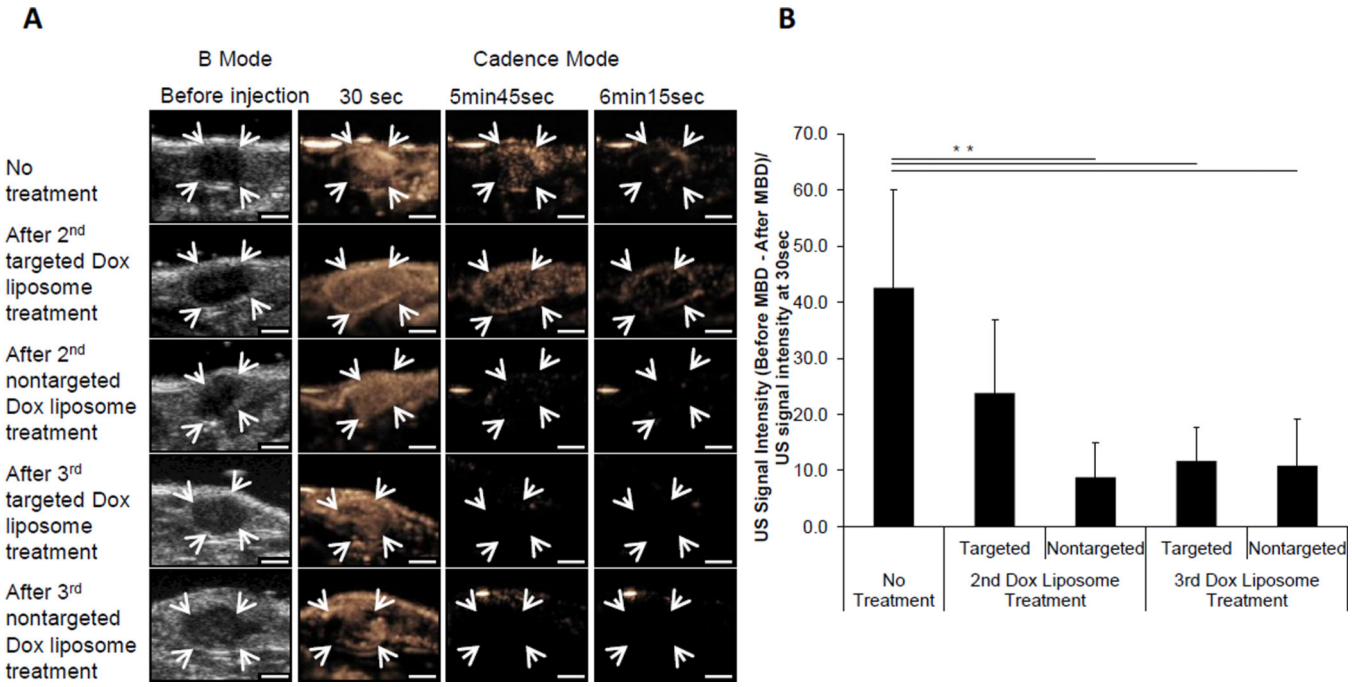

Figure 7.

The availability of NRP on the tumor vasculature was studied by injecting NRP-targeted (C-LPP) microbubbles and monitoring vascular accumulation with ultrasound (US), similar to [30, 31]. (A) US images of tumors after C-LPP microbubble injection: a B-Mode image was used to define the tumor region of interest, an image acquired at 30 sec after C-LPP microbubble injection validates tumor perfusion, an image acquired at 5 min 45 sec after injection is used to visualize binding of C-LPP microbubbles on the tumor vasculature, and an image acquired at 6 min 15 sec after injection is acquired to visualize remaining circulating C-LPP microbubbles after a destructive pulse (which occurred at 6 min after injection). (B) The difference between the image intensity at 5 min 45 sec (before MBD) and 6 min 15 sec (after MBD) was used to characterize the binding of the C-LPP microbubbles onto the tumor vasculature. The binding of the C-LPP microbubbles to the endothelium was reduced after the treatments. ** $p<0.01$.

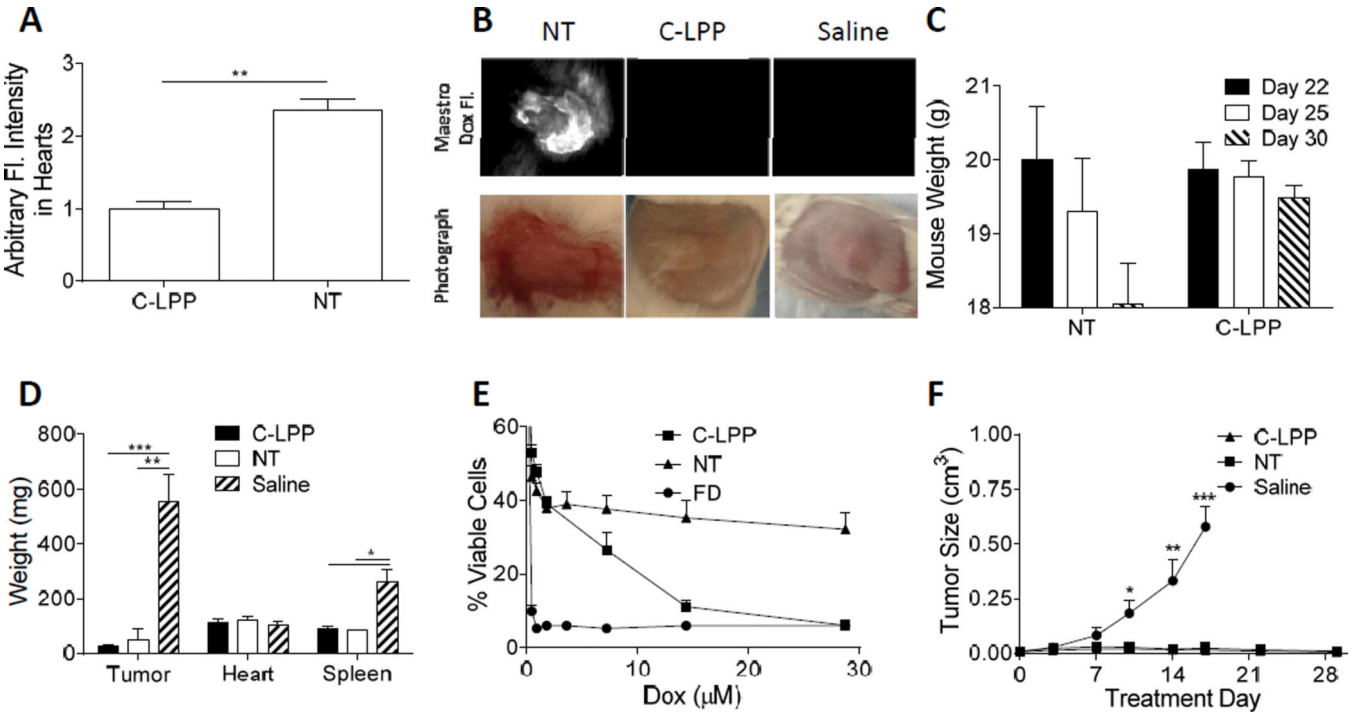

Figure 8.

Toxicity and efficacy of doxorubicin (Dox)-loaded carboxyl-terminated NRP-targeted liposomes (C-LPP liposomes), as compared to non-targeted (NT) liposomes, against NDL tumor cells both *in vitro* and *in vivo*. (A) *Ex vivo* measurements for Dox in heart tissue were performed 24 hr following the final liposomal treatment. (B) Maestro fluorescence images and photographs of skin demonstrate Dox accumulation and toxicity after injection of Dox loaded liposomes over 28 days. (C) Mouse weight over the final week of treatment. (D) *Ex vivo* tissue weights at termination of study (17 days for saline, 29 days for NT and C-LPP-liposome group). (E) MTT assay of NDL cells cultured *in vitro* treated with liposomal and free Dox (FD) for 72 hr, 0.63 mol% C-LPP liposomes effectively inhibited cell growth as compared to NT liposomes. (F) Tumor growth as a function of days post initiation of Dox treatment (saline control mice were sacrificed at 17 days due to large tumor size, as measured by ultrasound imaging). * $p<0.05$, ** $p<0.01$, *** $p<0.001$.